Chinese Journal of
POLYMER SCIENCE

RESEARCH ARTICLE

https://doi.org/10.1007/s10118-026-3646-1
Chinese J. Polym. Sci. **2026**, *44*, 1716–1726

Pre-Twist-dependent Configurations of Hydrogel Rings and Their Distinct Modes of Self-sustained Locomotion

Han-Lei Cheng[a], Qing-Li Zhu[a], Zhi-Jian Wang[a*], Josef Breu[b*], and Zi-Liang Wu[a*]

[a] *Department of Polymer Science and Engineering, Zhejiang University, Hangzhou 310058, China*
[b] *Bavarian Polymer Institute and Department of Chemistry, University of Bayreuth, Bayreuth 95440, Germany*

Electronic Supplementary Information

Abstract Self-sustained continuous motion is a central functional objective in soft actuators and robotics. One key challenge lies in establishing a persistent, self-regulated deformation feedback in soft materials under external stimulation, which is ultimately rooted in their geometry and configuration. Here, based on a cylindrical hydrogel with fast, reversible, and anisotropic photoresponsiveness, we construct a series of hydrogel rings by twisting one end of the gel string and closing it into a loop. By regulating the built-in twist (*Tw*) and the resulting internal prestress, the rings adopt distinct configurations that give rise to multiple motion modes under light irradiation. Gel rings with relatively small *Tw* remain in quasi-flat configurations and display coupled rolling and spinning motions. As *Tw* increases, the rings undergo Michell's instability and rapidly snap into a figure-of-eight configuration upon light irradiation, subsequently exhibiting irregular tumbling motions. At even larger *Tw*, the rings adopt "dough twist" configurations, showing persistent rolling under constant irradiation. Distinct motion modes arise from different actuation-deformation feedback loops established in hydrogels with distinct configurations and stress distributions. These results demonstrate not only the role of the configuration in governing locomotion, but also the potential of a single hydrogel system to achieve diverse motion behaviors through programming internal stresses.

Keywords Topological structures; Ring topology; Self-regulated motions; Anisotropic hydrogels; Feedback loops

Citation: Cheng, H. L.; Zhu, Q. L.; Wang, Z. J.; Breu, J.; Wu, Z. L. Pre-twist-dependent configurations of hydrogel rings and their distinct modes of self-sustained locomotion. *Chinese J. Polym. Sci.* **2026**, *44*, 1716–1726.

INTRODUCTION

Self-sustained motion is a fundamental requirement for soft robots with physical intelligence.[1–3] Such capability underpins autonomous functions, from locomotion to adaptive task execution in complex and unstructured environments.[4–8] To achieve such self-sustained motion without reliance on onboard power supplies or centralized control systems, one common strategy is to employ responsive materials that can undergo cyclic deformation in response to external stimuli and consequently generate locomotion.[8–16] Early soft robotic systems based on responsive materials typically adopted this strategy, in which cyclic deformation was imposed through carefully timed or spatially modulated external stimuli such as heat and light.[13–16] In contrast, an alternative and increasingly attractive strategy embeds the control logic directly into the structure through geometric design.[17–23] In such systems, deformation itself establishes a self-regulating feedback loop, enabling sustained motion to emerge under simplified, or even constant, stimulations.

Properly designed configurations can allow self-shadowing, geometric symmetry breaking, and energy dissipation to operate synergistically, giving rise to a closed deformation feedback loop that enables self-sustained motion. Several studies have demonstrated this principle.[24–33] A representative example is our previous work on an anisotropic cylindrical hydrogel, which exhibits self-regulated, continuous rolling under constant light irradiation.[26] Yin *et al*. also reported a defected twisted liquid crystal elastomer ring topology capable of autonomous periodic flip-spin-orbit motion under constant temperature or light.[20,29,30] In addition, we also reported several hydrogel-based soft robots with knotted structures (*e.g.*, trefoil knots and Solomon links) capable of continuous rolling and rotation motions under static light irradiation.[31–33] These motions originate from photothermally induced symmetry-breaking that is sustained by fast, reversible deformation to continuously refresh the irradiated region, thereby closing the deformation feedback loop. This principle enhances the design of autonomous soft robots and broadens their applicability across diverse environments and tasks.[20]

* Corresponding authors, E-mail: wangzhijian@zju.edu.cn (Z.J.W.)
E-mail: Josef.Breu@uni-bayreuth.de (J.B.)
E-mail: wuziliang@zju.edu.cn (Z.L.W.)
Special Topic: Functional Gels
Received January 31, 2026; Accepted March 9, 2026; Published online May 14, 2026

Although topological and geometric designs establish a foundational route to self-sustained motion, additional design dimensions to introduce richer deformation pathways and feedback mechanisms are required to further increase motion complexity. In this context, ring-shaped responsive materials with different internal torsions show distinct three-dimensional (3D) configurations with specific stress distributions. The different configurations may establish distinct deformation feedback loops and result in diverse modes of self-sustained motion under constant external stimuli.[32,34]

In this study, we use hydrogel ring as a model and investigate how preset torsion embedded in the gel ring governs its configuration and motion behavior under light stimulation. The gel rings are constructed by pre-twisting a cylindrical hydrogel and subsequently closing it into a loop (Fig. 1a). The hydrogel has an anisotropic structure and fast responses to temperature and light irradiation. By varying the built-in twist (*Tw*), the gel rings adopt distinct configurations, ranging from a quasi-flat shape to a figure-of-eight configuration, and finally to a highly twisted closed-loop morphology referred to as the "dough twist" configuration (Fig. 1b). Upon light irradiation, the illuminated region of the hydrogel undergoes rapid anisotropic deformation, which is transmitted to induce global deformation of the structure. Owing to the distinct feedback loops established in the gel rings with different configurations, the localized response is continuously regenerated, giving rise to self-sustained deformation and locomotion. The gel rings with the same topology yet different configurations exhibit distinct modes of motion, including coupled rotation and spinning, tumbling, and rolling (Fig. 1c). These results demonstrate not only the critical role of built-in twist in governing the configuration and locomotion of the gel ring, but also the potential of a single system to achieve diverse motion behaviors by programming the internal stresses.

EXPERIMENTAL

Synthesis of Anisotropic Light-responsive Hydrogels

An anisotropic light-responsive hydrogel containing charged nanosheets, which exhibited fast and isochoric responses driven by temperature-mediated electrostatic repulsion between the nanosheets, was employed to fabricate the hydrogel rings. Specifically, a cylindrical poly(*N*-isopropylacrylamide) (PNIPAm) gel incorporating randomly dispersed gold nanoparticles (AuNPs) and highly aligned fluorohectorite $[Na_{0.5}]^{inter}[Li_{0.5}Mg_{2.5}]^{oct}[Si_4]^{teter}O_{10}F_2$ nanosheets (NSs) was prepared *via* the flow-induced alignment of NSs in the precursor solution, followed by *in situ* photopolymerization (Fig. 1a). The precursor solution was prepared by dissolving monomer *N*-isopropylacrylamide (NIPAm, 10.1 wt%), crosslinker *N,N'*-methylenebisacrylamide (MBAA, 0.3 wt%), and photo-initiator lithium phenyl-2,4,6-trimethylbenzoylphosphinate (LAP, 0.1 wt%) in an aqueous suspension containing photothermal AuNPs (0.5 wt%) and charged NSs (1.0 wt%). The homogeneous precursor solution was then injected into transparent soft rubber tubes (inner diameter=2.0 mm) at a constant flow rate of 10

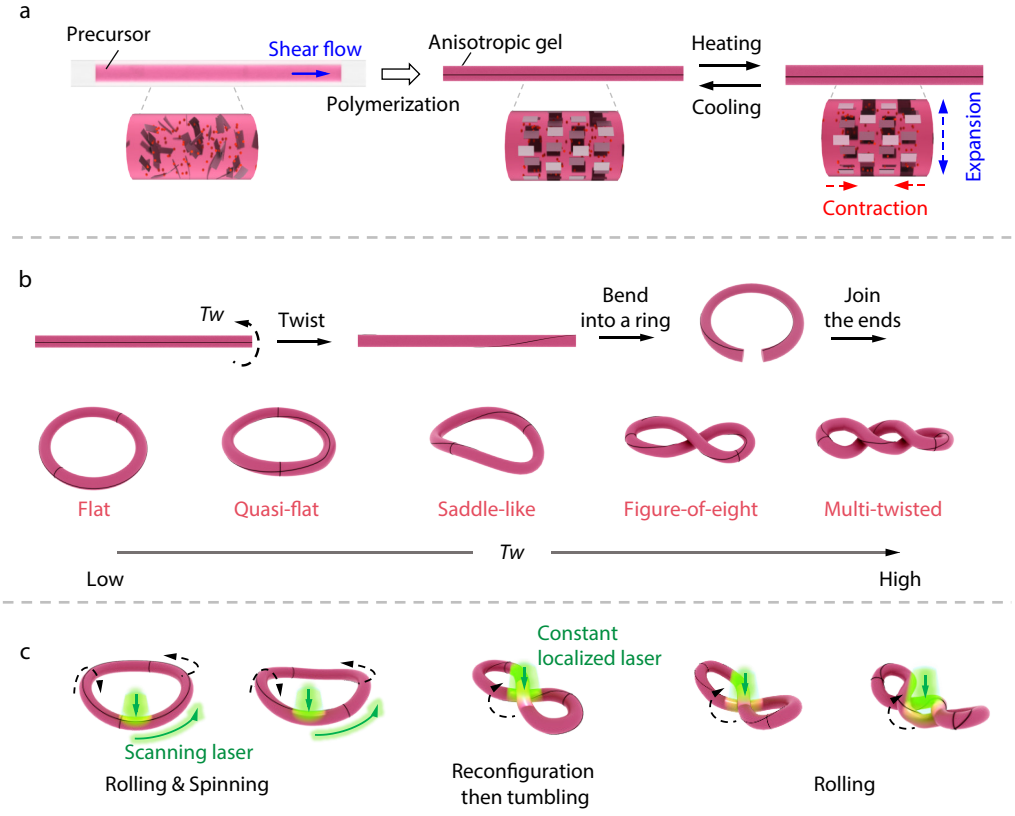

Fig. 1 Illustration of fabrication, configuration programming, and light-driven locomotion of hydrogel rings with diverse built-in twists (*Tw*). (a) Preparation and anisotropic responsive deformation of a cylindrical hydrogel with concentric alignment of nanosheets; (b) Distinct configurations of the gel rings by introducing various *Tw*; (c) Multiple locomotion behaviors of the gel rings under appropriate light irradiation.

https://doi.org/10.1007/s10118-026-3646-1

mm·s^{-1}, which induced the alignment of NSs along the flow direction. Immediately after injection, the filled tubes were exposed to ultraviolet (UV) light (365 nm) for 120 s to initiate photopolymerization, yielding anisotropic cylindrical PNIPAm gels with uniformly aligned NSs (Fig. S1 in the electronic supplementary information, ESI). To remove residual unreacted species and reach swelling equilibrium, the as-prepared gels were subsequently immersed in a large excess of deionized water at room temperature.

Fabrication and Light-driven Motion of Hydrogel Rings

After reaching swelling equilibrium, the cylindrical PNIPAm hydrogel with a diameter of 2.0 mm and a typical length of 50 mm (varying from 30 mm to 80 mm in some experiments) was prepared. The cylindrical gel was then mechanically twisted to a predefined twist by hand. The two ends were then bonded using a low-interference soft adhesive to form a closed ring. By varying the built-in twist *Tw*, gel rings with the same topology yet different configurations were fabricated. To enable precise control of the applied pre-twist and facilitate clear identification of the rings, a black reference line parallel to the central axis of the cylindrical gel was marked along the surface prior to twisting.

For light-driven actuation, the gel rings were placed on a flat poly(vinyl chloride) substrate submerged in a water bath at room temperature and irradiated with a laser source (wavelength: 520 nm) at a prescribed intensity. The light source was positioned approximately 30 cm from the sample, producing an illumination spot with a diameter of about 15 mm. Gel rings with different configurations exhibited distinct dynamic shape transformations and locomotion behaviors under continuous illumination. These responses were recorded as photographs or videos using a digital camera equipped with a long-pass cut-off filter (550–1100 nm) to eliminate interference from the incident green light.

Pre-Twist-controlled Configurations of Hydrogel Rings

We first demonstrate that cylindrical hydrogels with different built-in twists (*Tw*) adopt distinct configurations after being closed into loops, arising from the internal stress introduced by pre-torsion (Fig. 2a). Unless otherwise specified, hydrogels of 2.0 mm in diameter and 50 mm in length were adopted. When *Tw*=0, corresponding to a twist-free state, the hydrogel maintains a flat circular shape. As the imposed *Tw* increases to 2π, the ring exhibits slight warping while remaining largely planar. When *Tw* reaches 4π, the accumulated torsional energy increases, and the ring deforms into a saddle-like configuration, accompanied by a pronounced increase in out-of-plane deformation. In this regime, the ring enters a bistable state, in which the circular configuration can be driven into the figure-of-eight configuration by external stimuli such as mechanical force or light (Fig. 2b). Once formed, each configuration retains after the stimuli are removed. When *Tw* exceeds a critical value ($Tw > Tw_c \approx 4\pi$), the ring undergoes a spontaneous instability and snaps into a figure-of-eight configuration *via* Michell's instability. According to the mechanical instability theory and our previous work, when the length-to-diameter ratio (*L*/*D*) of the gel ring exceeds 15, the critical twist Tw_c is primarily governed by the ratio of torsional stiffness to bending stiffness of the material and becomes essentially independent of ring size.[32,34,35] In the present study, the adopted gel has $L/D \geq 15$ and exhibits a critical twist of $Tw_c \approx 4\pi$. When this threshold is exceeded, Michell's instability occurs through out-of-plane buckling, which relaxes the accumulated torsion energy at a lower cost of the bending energy. In this supercritical regime, the figure-of-eight configuration becomes an energy-minimized monostable state: even if the ring is forcibly deformed back into a circular flat shape, it spontaneously returns to the figure-of-eight configuration after the external constraint is released. Such monostable and bistable topological transitions in twisted elastic rings have been reported in our previous work and in related studies.[32] With a further increase in *Tw* from 5π to 8π, substantial torsional energy accumulates in the twisted cylindrical gel. After the twisted gel is bonded into a ring and the external constraint is removed, the gel ring rapidly deforms into a "dough twist" configuration characterized by multiple self-contact points. This deformation instability enables the system to relax more stored torsional energy and reach a lower-energy state.

Configuration-dependent Self-sustained Motion Modes

We then show that hydrogel rings with different configurations exhibit distinct self-sustained motion modes under appropriate light irradiation conditions. A straight cylindrical PNIPAm gel containing aligned charged nanosheets (NSs) and photothermal gold nanoparticles (AuNPs) undergoes rapid anisotropic deformation, accompanied by pronounced changes in mechanical stiffness under uniform heating or light irradiation (Fig. 1a and Fig. S2 in ESI). When the temperature exceeds the lower critical solution temperature of PNIPAm, dehydration of the polymer chains occurs, leading to the removal of bound water and an increase in the effective dielectric permittivity of the medium.[36–41] This enhanced permittivity strengthens the electrostatic repulsion between the aligned charged nanosheets and increases their intersheet spacing.[40] Consequently, upon heating, the gel undergoes rapid anisotropic deformation, expanding perpendicular to the nanosheet alignment by 1.08 while contracting along the alignment direction by 0.87 within about 5 s; this deformation is fully reversible upon cooling. Owing to the photothermal effect of the embedded AuNPs, similar deformation behavior can be achieved under light irradiation (Fig. S3 in ESI). By leveraging this cylindrical gel with fast, reversible, and anisotropic responsiveness, a variety of locomotion behaviors can be achieved under simple and constant stimulation. In our previous work, such straight cylindrical gels were shown to undergo continuous rolling motion under constant light irradiation.[26] When the same material is reconfigured into ring-shaped architectures, the introduction of topological constraints fundamentally alters the deformation-motion coupling.[31,32,34] As a result, distinct self-sustained locomotion modes emerge in the gel rings *via* topological design.

We first investigated the response of a flat gel ring without any pre-twist under constant laser irradiation and found that localized light exposure does not induce locomotion (Figs. 3a, 3b and Movie S1 in ESI). Only localized inward rolling is observed, with an inward rolling angle α reaching a maximum of approximately 75°, whereas the global rotation angle β and the center-of-mass displacement *s* are negligible, indicating the absence of any net spinning or tumbling motion. When a

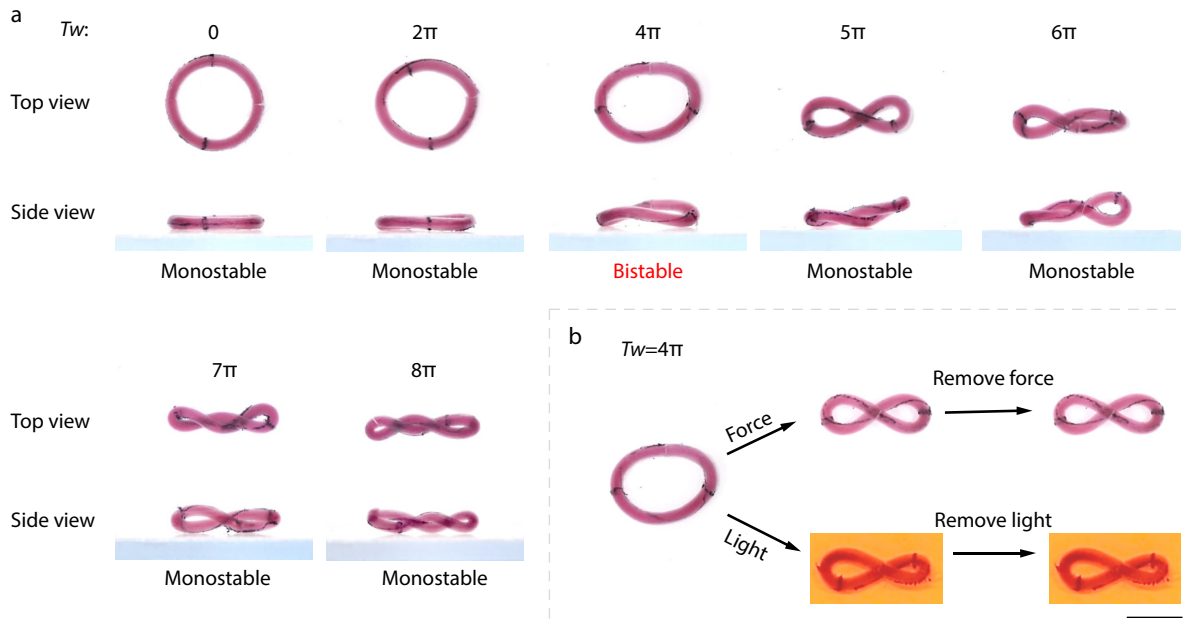

Fig. 2 Pre-twist-dependent configurations and bistable behavior of the hydrogel rings. (a) Photographs of the gel rings with different built-in twists (*Tw*), shown in both top and side views; (b) Photographs showing that the gel ring with *Tw*=4π displays two stable configurations. Scale bar, 10 mm.

fixed point on the ring is irradiated from above, the limited penetration depth of light establishes a pronounced photothermal gradient across the thickness of the gel. This gradient induces a corresponding strain mismatch: the illuminated top surface undergoes heating-induced contraction, whereas the cooler, non-illuminated bottom region remains essentially undeformed.[26,27,31] As a result, an eccentric resultant force is generated, leading to localized bending deformation. Despite the presence of this local stress asymmetry, both the deformation and the associated torque remain highly confined to the irradiated region. The resulting inward bending is insufficient to initiate the global rolling of the ring, nor can it overcome the gravitational load of the surrounding non-irradiated segments to induce tumbling of the entire structure. Consequently, the gel ring only transitions from a flat configuration to a slightly warped state (Fig. 3d). Increasing the light intensity does not change this behavior.

To overcome the limitation of localized actuation, we employed a dynamic scanning illumination strategy, in which a focused light spot is swept circumferentially along the ring in the counterclockwise direction at a constant angular velocity (laser intensity: 4.5 W·cm^{-2}; scanning speed: 51.4 (°)·s^{-1}). In this mode, the gel ring with *Tw*=0 exhibits continuous inward rolling accompanied by a counterclockwise spinning motion, while the overall ring adopts a saddle-like configuration (Figs. 3c, 3e and Movie S1 in ESI). The ring undergoes inward rolling with α reaching approximately 600° within about 20 s, corresponding to an average rolling rate α' of about 30 (°)·s^{-1}, while simultaneously exhibiting a global rotation with β increasing to about 20° (average rotation rate $\beta' \approx 1$ (°)·s^{-1}) about its center. Notably, during this motion, no obvious net translational displacement of the ring center is observed. Such deformation arises from a deformation feedback loop generated by dynamic scanning illumination. Each segment of the ring is periodically irradiated and subsequently allowed to cool and recover, generating a traveling zone of inward bending that is synchronized with the scanning light spot. This repeated inward deformation and recovery gives rise to sustained inward rolling of the ring, while simultaneously producing a spinning motion along the scanning direction of the light. The spinning motion also originates from the asymmetric forces generated during the local deformation-recovery cycle: as the light spot moves, the associated force imbalance follows, biasing frictional interactions with the substrate and resulting in directional propulsion.[31] Although the instantaneous spinning direction may exhibit stochastic fluctuations, the overall, time-averaged spinning motion remains aligned with the scanning direction of the light. Inverting the scanning direction reverses the net spinning direction. When the built-in twist *Tw* is increased to π or 2π, the overall locomotion mode of the gel ring remains unchanged under dynamic scanning, and neither the rolling nor the spinning velocity varies significantly. This indicates that the locomotion dynamics of the quasi-flat ring are insensitive to moderate variations in the pre-torsion magnitude under dynamic scanning irradiation. Notably, the laser scanning speed critically affects the actuation behavior (Fig. S4 in ESI). When the scanning is too fast, the local temperature rise is insufficient to induce strong hydrogel contraction, resulting in inadequate driving force to overcome friction. Conversely, excessively slow scanning leads to heat accumulation and weakens the dynamic temperature gradient required for continuous motion.[42] Therefore, a balanced scanning speed that couples photothermal heating with heat dissipation is required to achieve stable actuation.

When the built-in twist *Tw* of the hydrogel ring reaches 4π, the embedded torsion drives the gel ring into a saddle-like configuration. At this twist level, *Tw* approaches the critical

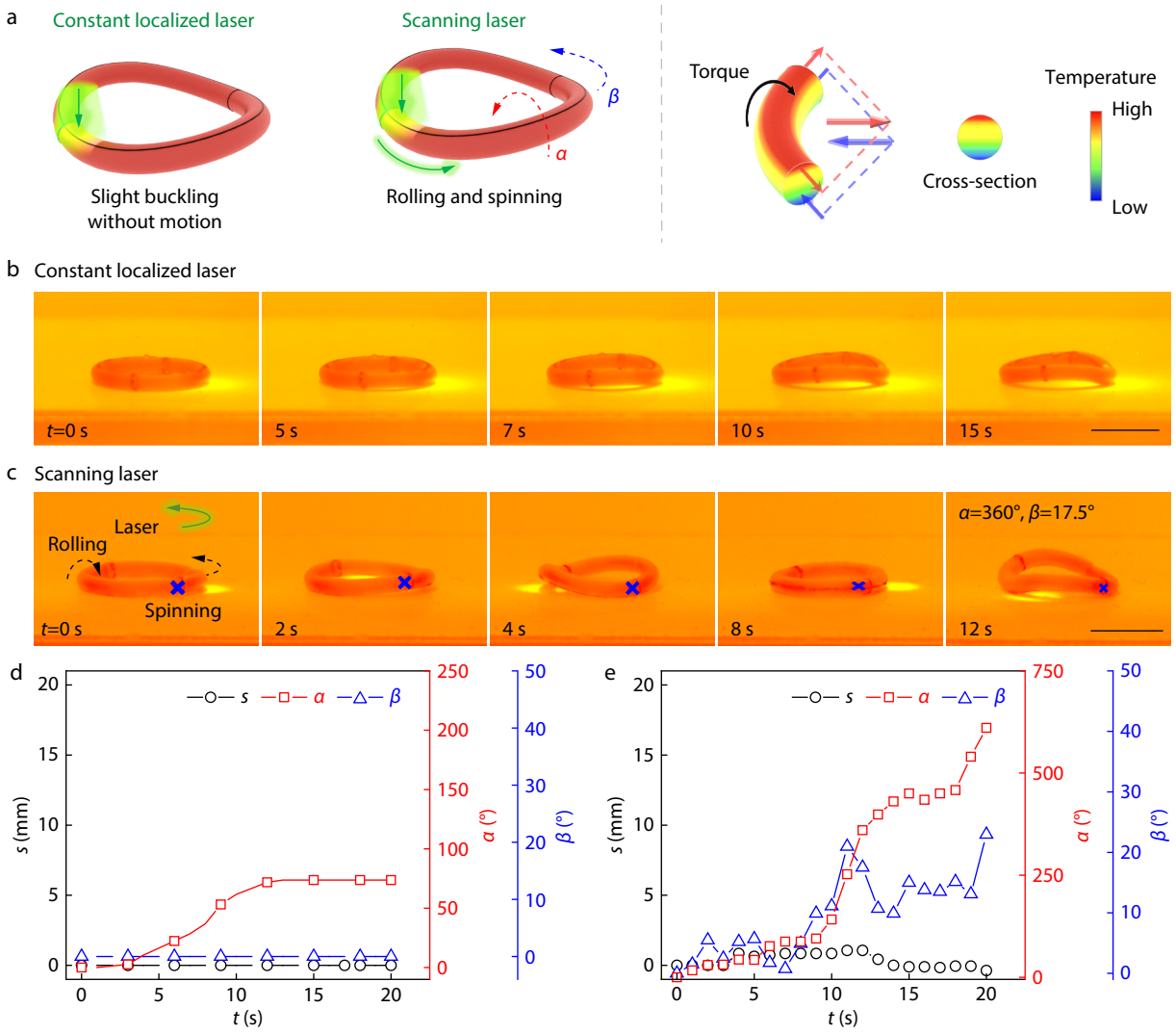

Fig. 3 Locomotion of the hydrogel ring with *Tw*=0 under varied irradiation conditions. (a) Schematic for the morphing and motion of the gel ring under different light irradiation conditions; Snapshots of the gel ring under (b) constant laser irradiation and (c) scanning laser irradiation at different illumination times; Time evolution of the center-of-mass displacement *s*, rolling angle *α*, and spinning angle *β* of the gel ring under (d) constant localized laser and (e) scanning laser stimulation. Concentration of AuNPs, 0.5 wt%; sample length, 50 mm; sample diameter, 2.0 mm; laser intensity, 4.5 W·cm^{-2}. Scale bar, 10 mm.

value Tw_c required to trigger Michell's instability.[32,34,35] Consequently, under scanning light irradiation, the ring first deforms into the figure-of-eight state *via* Michell's instability due to the change in mechanical stiffness and the resultant decrease in Tw_c. However, in this figure-of-eight configuration, dynamic scanning illumination can no longer induce regular or sustained motions. The deformation becomes spatially delocalized and mechanically self-constrained, preventing the establishment of a stable deformation feedback loop under moving light. To activate self-sustained motion, we instead apply stationary, uniform illumination focused on the self-contact region of the gel ring. Interestingly, under this localized and constant optical stimulus, the ring exhibits a continuous tumbling motion without a fixed tumbling direction (Fig. 4 and Movie S2 in ESI). During motion, the gel ring maintains its overall figure-of-eight configuration. Remarkably, despite this overall topological stability, the position of the self-contact point undergoes pronounced migration along the hydrogel string, accompanied by severe out-of-plane deformation. Concurrently, the gel ring bends toward the light driven by the strain gradient across the thickness, while a finite lateral bending results from the structural asymmetry of the configuration. This asymmetric bending breaks the collinearity between the gravitational and support reaction forces, thereby generating a net torque that drives the gel ring to tumble toward the bending direction. Crucially, the deformation and motion dynamically refresh the illuminated regions because of the self-shadowing effect: areas that were previously heated rotate into shadow and cool, while regions that were initially shaded move into the light and begin to contract (Fig. S5 in ESI). This process establishes an autonomous deformation-illumination feedback loop that prevents the system from reaching a static equilibrium and thus enables continuous locomotion.[35,43–46] However, at *Tw*=4π,

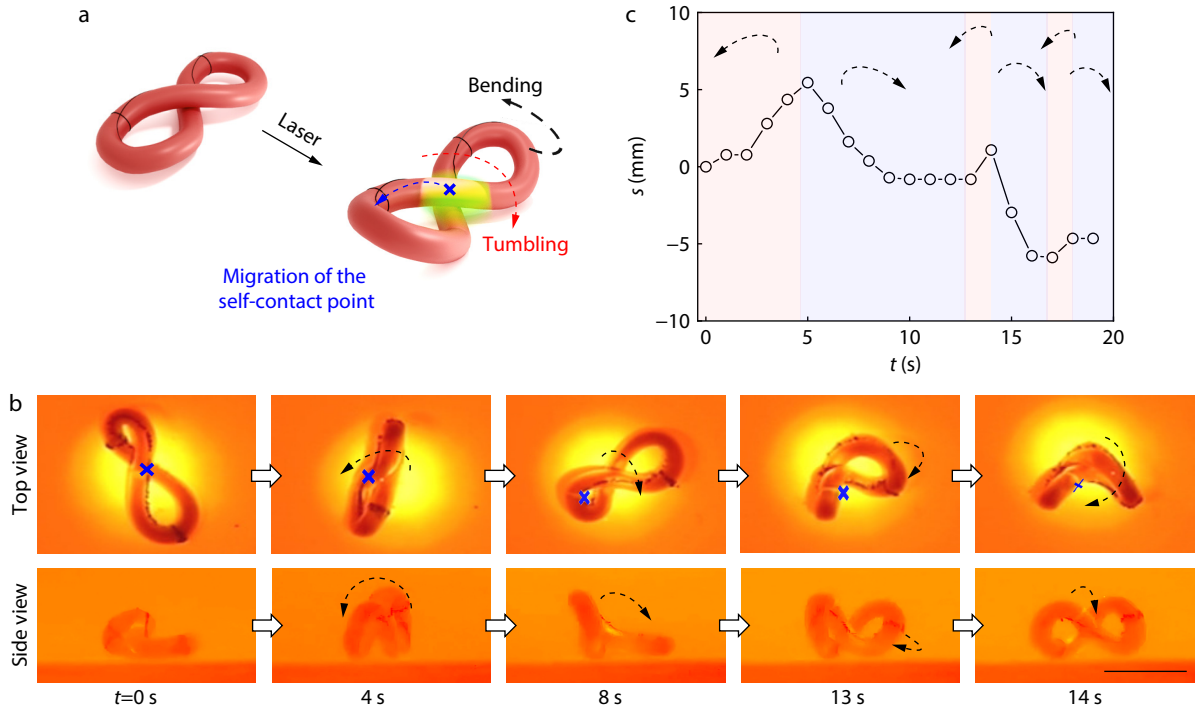

Fig. 4 Irregular tumbling of a figure-of-eight hydrogel ring with *Tw*=4π reconfigured from a saddle-shaped configuration under constant laser irradiation. (a) Schematic for the light-induced deformation and tumbling motion of the gel ring, highlighting laser-induced bending and the migration of the initial self-contact point; (b) Snapshots of the gel ring under constant laser irradiation. Concentration of AuNPs, 0.5 wt%; sample length, 50 mm; sample diameter, 2.0 mm; laser intensity, 3.4 W·cm^{-2}. Scale bar, 10 mm. (c) Displacement of the gel ring, *s*, as a function of irradiation time, *t*. Arrows indicate different tumbling directions.

the tumbling direction is unstable, irregular, and can occur in multiple spatial directions, exhibiting omnidirectional randomness. This is because the ring exhibits a relatively loose topological winding due to the small pre-torsion, which endows it with a higher degree of freedom for deformation. The resulting structural slackness facilitates sliding at the self-contact point and allows large-amplitude out-of-plane deformations without a fixed direction, causing the tumbling direction to remain non-persistent. Tracking the displacement of the ring's center of mass reveals a complex and irregular trajectory, manifested as aperiodic fluctuations in the displacement-time curve.

In contrast, a ring with a higher pre-twist *Tw* (≥ 5π), which stably adopts a highly twisted configuration, exhibits more regular tumbling behavior when the central region is illuminated (Fig. 5a and Movie S3 in ESI). Although occasional stochastic reversals in the rolling direction may occur during the early stages (within the first few seconds) under vertical light irradiation, the overall tumbling direction remains stable (Figs. 5b and 5c). The initial rolling direction instability is likely due to the relatively slow initial rolling speed: upon illumination, the ring bends upward and may randomly topple to one side, while the constraints imposed by the gel ring's ends suppress instantaneous velocity, causing momentary stalls. With continued light irradiation, the gel ring gradually accelerates, and once sufficient kinetic inertia is established, the rolling direction stabilizes, and the speed reaches a steady state. In addition, despite the increased geometric complexity induced by the higher pre-twist, the tighter topological winding enforces strong self-constraints that promote a high degree of structural self-similarity during motion. In particular, the self-contact point exhibits negligible displacement. This enhanced self-similarity stabilizes the deformation feedback loop that is essential for self-regulated continuous actuation.[47]

Owing to this stable rolling, the angular velocity (ω) can be used to quantify the rolling motion behavior of the ring. For example, at *Tw*=6π, with continued irradiation, the gel ring gradually accelerates, eventually reaching a steady-state rolling speed ω_{max} of up to 16 (°)·s^{-1} (Fig. 5d). Furthermore, as the built-in twist *Tw* is increased from 5π to 8π, the maximum equilibrium rolling speed ω_{max} also increases (Fig. 5e). This trend can be attributed to the enhanced spatial self-confinement at higher twists, which suppresses excessive bending and accelerates the refresh rate of the illuminated region. As a result, the deformation feedback loop is strengthened, leading to faster rolling motion.

To achieve a more stable rolling direction even at the initial stage of motion, oblique illumination proves effective (Fig. S6 in ESI). Under 45° oblique illumination, the gel rings exhibit more stable rolling or directional motion toward the incident light direction. Similarly, the maximum equilibrium rolling speed increases with increasing pre-twist *Tw*. However, the rolling speeds are slightly lower than those observed under vertical illumination. This reduction is attributed to the smaller through-thickness photothermal gradient under oblique irradiation, together with the larger lateral bending angle induced by tilted light incidence, which collectively hinder rolling motion. Notably, under oblique illumination, the driving force is insufficient to sustain motion at *Tw*=8π due to

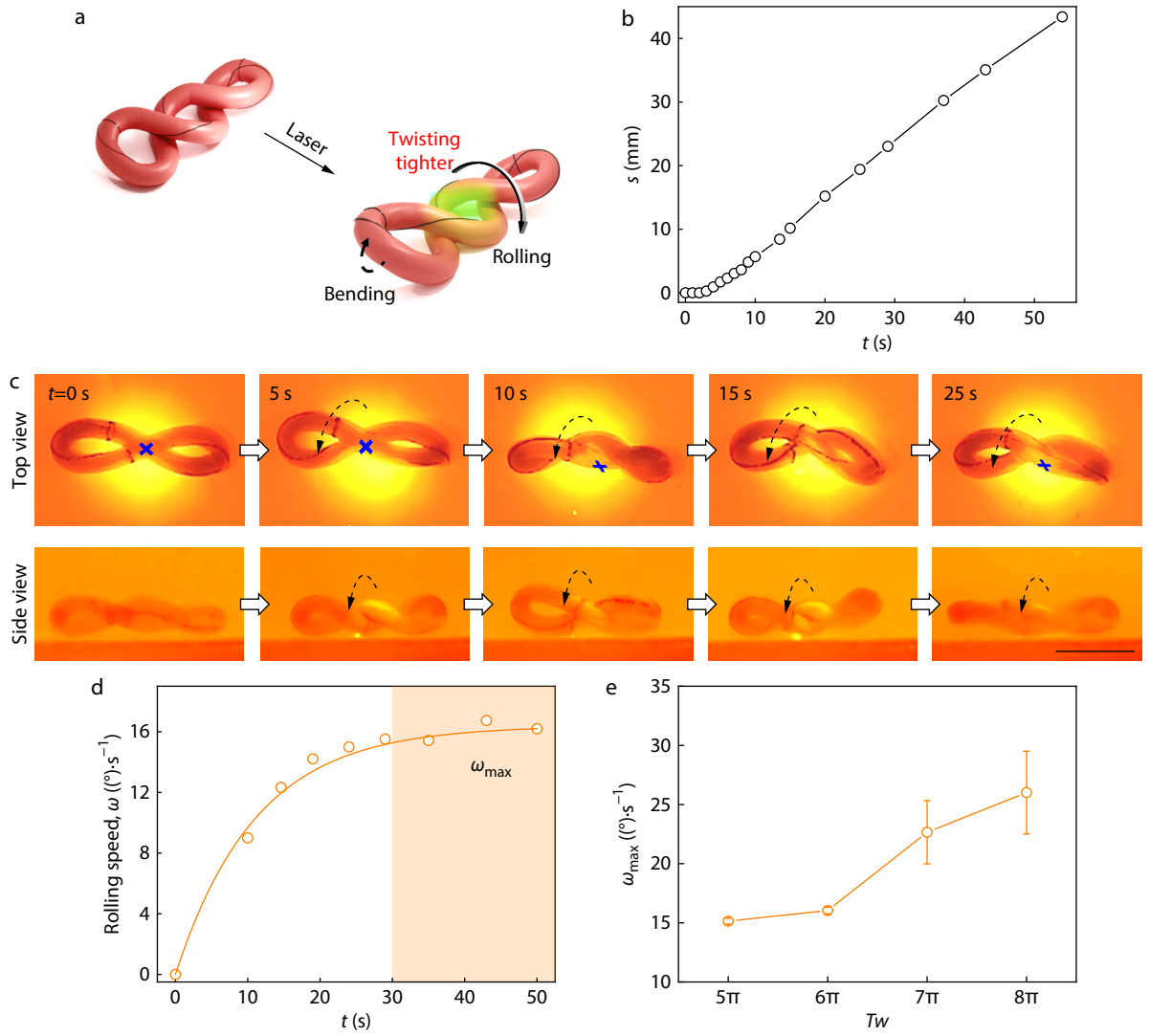

Fig. 5 Rolling of the hydrogel rings with a "dough twist" configuration under constant laser irradiation. (a) Schematic for the light-induced deformation and rolling motion of the gel ring with a high built-in twist of *Tw*=6π, spontaneously forming tightly twisted configuration; (b) Representative displacement (*s*) of the gel ring with *Tw*=6π as a function of irradiation time, *t*; (c) Snapshots of the gel ring with *Tw*=6π under constant laser irradiation. Scale bar, 10 mm. (d) Rolling angular speed (ω) as a function of irradiation time, *t*; (e) Maximum rolling angular velocity (ω_{max}) as a function of the pre-twist (*Tw*) under constant laser irradiation. Concentration of AuNPs, 0.5 wt%; sample length, 50 mm; sample diameter, 2.0 mm; laser intensity, 3.4 W·cm^{-2}.

the higher frictional resistance in this configuration. These results collectively highlight the critical role of the configuration in determining the motion mode. To facilitate a clearer understanding of the relationships among the configurations, a summary table is provided in the Supporting Information (Table S1 in ESI) to summarize the stimulation mode, motion type, and key performance metrics.

Interplay of Geometric and Stimulus Parameters in Motion Regulation

The above work demonstrates that hydrogel rings with different pre-twists *Tw* exhibit distinct motion modes under laser irradiation, ranging from spinning-like deformation under dynamic scanning irradiation to irregular tumbling and ultimately to stable rolling under continuous light irradiation. While this work primarily focuses on the role of the pre-twist in governing configuration and deformation, several additional parameters also significantly influence the rolling performance. Taking *Tw*=6π as a representative case, the actual twisting density of the ring is determined by the length of the cylindrical gel from which it is fabricated (Figs. 6a and 6b). For gel rings with the same built-in twist, smaller ones are more difficult to actuate. In this regime, the ring is almost entirely covered by the light spot, and stronger topological self-constraints further suppress the deformation and subsequent rolling motion.[48] Additionally, as the hydrogel length is increased to 50 mm, the rolling speed increases markedly, and continuous rolling is achieved. In contrast, excessively large rings exhibit diminished rolling performance: the increased bulky ends significantly raise the gravitational energy barrier for rolling, while the enlarged contact area with the substrate increases friction.[26] Based on these considerations, a hydrogel length of 50 mm was selected for the previous demonstration and subsequent investigation.

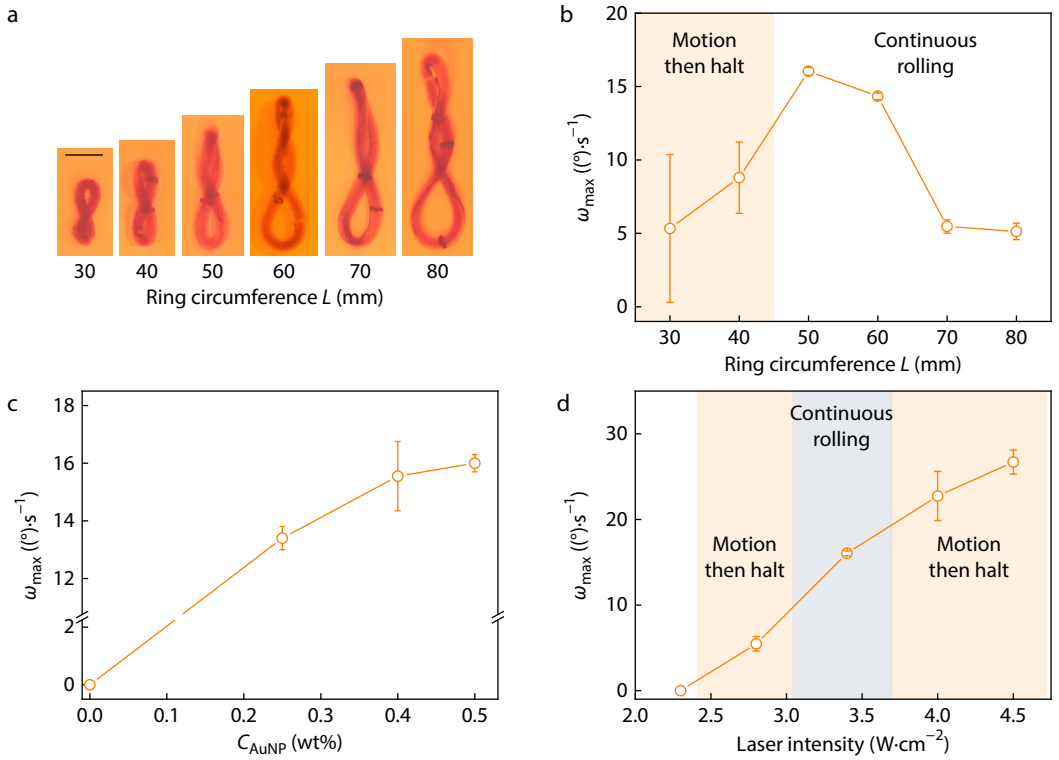

Fig. 6 Rolling behaviors of the hydrogel rings with *Tw* of 6π under constant laser irradiations. Snapshots of the gel rings with different circumferences (corresponding to different initial lengths *L* of gel strings) (a) and corresponding maximum rolling angular velocity (ω_{max}) (b); Concentration of AuNPs (C_{AuNP}), 0.5 wt%; laser intensity, 3.4 W·cm^{-2}. Scale bar, 10 mm. (c) ω_{max} of the gel rings as a function of C_{AuNP}. Sample length *L*, 50 mm; laser intensity, 3.4 W·cm^{-2}. (d) ω_{max} of the gel rings as a function of laser intensity. *L*, 50 mm; C_{AuNP}, 0.5 wt%.

In addition to geometric factors, the photothermal conversion capability of the hydrogel, which is governed by the concentration of AuNPs, also plays a critical role (Fig. 6c). In the absence of AuNPs, no motion is observed. When the AuNPs concentration is increased to 0.25 wt%, rolling motion emerges with a speed of approximately 13 (°)·s^{-1}, which further increases to about 16 (°)·s^{-1} at 0.5 wt%. Increasing the AuNPs concentration enhances the photothermal conversion efficiency of the gel ring, enabling a faster response to light stimulation and thereby improving the rolling performance.

Laser intensity is another key parameter that controls the motion behavior (Fig. 6d and Fig. S7 in ESI). Under low-intensity irradiation, the gel ring remains largely static due to the insufficient driving force arising from a weak photothermal gradient. When the laser intensity is increased to 3.4 W·cm^{-2}, sustained rolling motion is achieved. However, further increasing the intensity leads to rapid bending followed by a lateral roll of approximately 0.5π, after which the ring comes to a stop. This behavior is accompanied by excessive dehydration and contraction at elevated temperatures, which suppress deformation recovery and prevent the establishment of a stable deformation-motion feedback loop. Therefore, both excessively low and excessively high laser power densities are detrimental to sustained rolling. These results demonstrate that while the preset twist fundamentally determines the configurations and accessible deformation pathways, the size of the gel ring and photothermal conversion efficiency jointly tune the balance between driving torque and dissipation, thereby regulating rolling performance.

CONCLUSIONS

In summary, configuration can play a central role in establishing feedback loops that enable self-sustained motion in soft robots. This work demonstrates that both the configurations and motion modes of hydrogel rings can be elaborately tuned by controlling the built-in twist (*Tw*). As *Tw* increases, the gel ring undergoes a well-defined configuration evolution from quasi-flat to saddle-like shapes, followed by figure-of-eight and ultimately "dough twist" configurations. Different configurations require different stimulation schemes to realize self-sustained motion. In gel ring with a quasi-flat shape, dynamic scanning irradiation is necessary to induce rolling and spinning motions. Upon adopting a figure-of-eight configuration, either in response to stimulation or spontaneously, the gel ring exhibits continuous yet irregular tumbling under constant irradiation. In contrast, the "dough-twist" configuration displays stable rolling in a fixed direction under the same conditions. These behaviors originate from a dynamic, nonequilibrium coupling between fast, reversible photothermal deformation of the hydrogel and configuration-related self-shadowing, which together establish an actuation-deformation feedback loop under static light stimulation. Moreover, variations in the preset torsion subtly modulate the deformation magnitude and the associated feedback loops, thereby influencing the stability and speed of the resulting motion. By highlighting the decisive role of configuration in coordinating the stimulation mode and intensity, this work provides a versatile strategy for achieving diverse self-sustained motion behaviors within a single soft material system, offering new opportunities for the design of multimodal soft robots. Neverthe-

https://doi.org/10.1007/s10118-026-3646-1

less, the current system relies on a relatively high laser intensity to generate sufficient photothermal deformation and overcome the friction during locomotion. Future efforts aimed at improving photothermal efficiency, enhancing material sensitivity, and optimizing structural design may reduce the required energy input, enabling similar self-sustained motions under milder stimuli. This could further expand the potential applicability of these ring-shaped actuators in environmental exploration, targeted transport, and biomedical systems.

Conflict of Interests

The authors declare no interest conflict.

Electronic Supplementary Information

Electronic supplementary information (ESI) is available free of charge in the online version of this article at http://doi.org/10.1007/s10118-026-3646-1.

Data Availability Statement

The data that support the results of this study are available from the corresponding author upon reasonable request. Contact information of corresponding authors: wangzhijian@zju.edu.cn, Josef.Breu@uni-bayreuth.de, and wuziliang@zju.edu.cn.

ACKNOWLEDGMENTS

This study was financially supported by the National Natural Science Foundation of China (Nos. 52325302 and 524B1010).

REFERENCES

1 Chen, C.; Shi, P.; Liu, Z.; Duan, S.; Si, M.; Zhang, C.; Du, Y.; Yan, Y.; White, T. J.; Kramer-Bottiglio, R.; Sitti, M.; Iwasaki, T.; He, X. Advancing physical intelligence for autonomous soft robots. *Sci. Robot.* **2025**, *10*, eads1292.
2 Zhu, C.; Liu, B. Y.; Zhang, L. Z.; Xu, L. Autonomous soft robots: self-regulation, self-sustained, and recovery strategies. *Chinese J. Polym. Sci.* **2025**, *43*, 535–547.
3 Chung, T.; Choi, J.; Enomoto, T.; Park, S.; Kim, S.; Kim, Y. S. Self-regulating hydrogel actuators. *Chem. Rev.* **2025**, *125*, 9053–9088.
4 Yan, H.; Tang, P.; Li, S. H.; Zhao, T. Y.; Liu, M. J. Progress of biomimetic anisotropic poly(*N*-isopropylacrylamide) intelligent response actuators. *Chem. J. Chin. Univ. Chin.* **2020**, *41*, 936–946.
5 Zhang, X.; Zhou, Y.; Han, M.; Zheng, Y.; Liu, J.; Bao, Y.; Shan, G.; Yu, C.; Pan, P. Non-monotonic information and shape evolution of

Graphical Abstract

Pre-Twist-dependent Configurations of Hydrogel Rings and Their Distinct Modes of Self-sustained Locomotion

Han-Lei Cheng, Qing-Li Zhu, Zhi-Jian Wang, Josef Breu, and Zi-Liang Wu

Zhejiang University, China; University of Bayreuth, Germany

Programming built-in twist (*Tw*) in hydrogel rings generates distinct configurations with specific stress distributions, enabling multiple self-sustained motion modes: coupled rolling and spinning, irregular tumbling, and stable rolling. This work demonstrates that internal stress programming provides a versatile strategy for achieving diverse locomotion within a single soft material system.

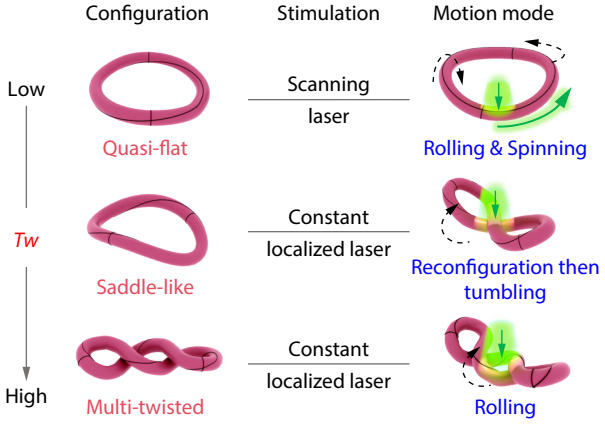

Chinese J. Polym. Sci. 2026, 44, 1716–1726 *https://doi.org/10.1007/s10118-026-3646-1*

polymers enabled by spatially programmed crystallization and melting. *Chem. Bio. Eng.* **2024**, *1*, 790–797.
6 Zhang, Y.; Liao, J.; Wang, T.; Sun, W.; Tong, Z. Polyampholyte hydrogels with pH modulated shape memory and spontaneous actuation. *Adv. Funct. Mater.* **2018**, *28*, 1707245.
7 Jian, Y.; Wu, B.; Le, X.; Liang, Y.; Zhang, Y.; Zhang, D.; Zhang, L.; Lu, W.; Zhang, J.; Chen, T. Anti-freezing and stretchable organohydrogels as soft actuators. *Research* **2019**, *2019*, 2384347.
8 Zhu, C. Y.; Lu, Y.; Jiang, L. X.; Yu, Y. L. Liquid crystal soft actuators and robots toward mixed reality. *Adv. Funct. Mater.* **2021**, *31*, 2009835.
9 Tian, L.; Tan, J. J.; Dong, W. L.; Yang, B.; Li, C. H.; Wang, D.; Huang, H. Y.; Li, X. T.; Zhu, C. Z.; Xu, J. Wireless autonomous soft crawlers for adjustable climbing actuation. *Chinese J. Polym. Sci.* **2023**, *41*, 405–413.
10 Luo, Z. B.; Cheng, W. Q.; Zhao, T. Y.; Xiang, N. Intelligent sensory systems toward soft robotics. *Appl. Mater. Today* **2024**, *37*, 102122.
11 Wang, X.-Q.; Ho, G. W. Design of untethered soft material micromachine for life-like locomotion. *Mater. Today* **2022**, *53*, 197–216.
12 Jung, Y.; Kwon, K.; Lee, J.; Ko, S. H. Untethered soft actuators for soft standalone robotics. *Nat. Commun.* **2024**, *15*, 3510.
13 Tang, Y. F.; Pan, F.; Qin, L.; Yu, Y. L. Adaptive locomotion of pleurotya caterpillar-inspired segmental crawling robots with multiple postures. *Adv. Funct. Mater.* **2025**, *35*, 2506987.
14 Wang, D.; Zhao, B.; Li, X.; Dong, L.; Zhang, M.; Zou, J.; Gu, G. Dexterous electrical-driven soft robots with reconfigurable chiral-lattice foot design. *Nat. Commun.* **2023**, *14*, 5067.
15 Palagi, S.; Mark, A. G.; Reigh, S. Y.; Melde, K.; Qiu, T.; Zeng, H.; Parmeggiani, C.; Martella, D.; Sanchez-Castillo, A.; Kapernaum, N.; Giesselmann, F.; Wiersma, D. S.; Lauga, E.; Fischer, P. Structured light enables biomimetic swimming and versatile locomotion of photoresponsive soft microrobots. *Nat. Mater.* **2016**, *15*, 647–653.
16 Wu, S.; Hong, Y.; Zhao, Y.; Yin, J.; Zhu, Y. Caterpillar-inspired soft crawling robot with distributed programmable thermal actuation. *Sci. Adv.* **2023**, *9*, eadf8014.
17 Zhang, L. Z.; Liu, B. Y.; Zhu, C.; Xu, L. Bioinspired actuation of liquid crystal elastomers with hierarchical structures based on light response. *Chinese J. Polym. Sci.* **2025**, *43*, 1981–1990.
18 Sitti, M. Physical intelligence as a new paradigm. *Extreme Mech. Lett.* **2021**, *46*, 101340.
19 Zhao, Y.; Li, Q.; Liu, Z.; Alsaid, Y.; Shi, P.; Jawed, M. K.; He, X. Sunlight-powered self-excited oscillators for sustainable autonomous soft robotics. *Sci. Robot.* **2023**, *8*, eadf4753.
20 Zhao, Y.; Chi, Y.; Hong, Y.; Li, Y.; Yang, S.; Yin, J. Twisting for soft intelligent autonomous robot in unstructured environments. *Proc. Natl. Acad. Sci. U.S.A.* **2022**, *119*, e2200265119.
21 Zhou, X.; Chen, G.; Jin, B.; Feng, H.; Chen, Z.; Fang, M.; Yang, B.; Xiao, R.; Xie, T.; Zheng, N. Multimodal autonomous locomotion of liquid crystal elastomer soft robot. *Adv. Sci.* **2024**, *11*, 2402358.
22 Kaspar, C.; Ravoo, B. J.; van der Wiel, W. G.; Wegner, S. V.; Pernice, W. H. P. The rise of intelligent matter. *Nature* **2021**, *594*, 345–355.
23 Shklyaev, O. E.; Balazs, A. C. Interlinking spatial dimensions and kinetic processes in dissipative materials to create synthetic systems with lifelike functionality. *Nat. Nanotechnol.* **2024**, *19*, 146–159.
24 Guo, H.; Li, K.; Yang, J.; Li, D.; Liu, F.; Zeng, H. Light-mediated communication in responsive materials ranging from individual self-oscillators to feedback-driven network. *Nat. Commun.* **2025**, *16*, 11315.
25 Ahn, C.; Li, K.; Cai, S. Light or thermally powered autonomous rolling of an elastomer rod. *ACS Appl. Mater. Interfaces* **2018**, *10*, 25689–25696.
26 Zhu, Q. L.; Cheng, H. L.; Liu, W. X.; Xiao, Y. B.; Wu, X. L.; Breu, J.; Hong, W.; Wang, Z. J.; Zheng, Q.; Wu, Z. L. Light-driven self-sustained rolling of cylinder hydrogels with fast and anisotropic responses. *Chinese J. Polym. Sci.* **2025**, *43*, 548–555.
27 Deng, Z.; Li, K.; Priimagi, A.; Zeng, H. Light-steerable locomotion using zero-elastic-energy modes. *Nat. Mater.* **2024**, *23*, 1728–1735.
28 Chen, F.; Xu, W.; Zhang, H.; Wang, Y.; Cao, J.; Wang, M. Y.; Ren, H.; Zhu, J.; Zhang, Y. F. Topology optimized design, fabrication, and characterization of a soft cable-driven gripper. *IEEE Robot. Autom. Lett.* **2018**, *3*, 2463–2470.
29 Chi, Y.; Li, Y.; Zhao, Y.; Hong, Y.; Tang, Y.; Yin, J. Bistable and multistable actuators for soft robots: structures, materials, and functionalities. *Adv. Mater.* **2022**, *34*, e2110384.
30 Qi, F.; Li, Y.; Hong, Y.; Zhao, Y.; Qing, H.; Yin, J. Defected twisted ring topology for autonomous periodic flip–spin–orbit soft robot. *Proc. Natl. Acad. Sci. U.S.A.* **2024**, *121*, e2312680121.
31 Zhu, Q. L.; Liu, W.; Khoruzhenko, O.; Breu, J.; Hong, W.; Zheng, Q.; Wu, Z. L. Animating hydrogel knotbots with topology-invoked self-regulation. *Nat. Commun.* **2024**, *15*, 300.
32 Zhu, Q. L.; Li, Z.; Cheng, H. L.; Liu, W. X.; Wang, Z. J.; Khoruzhenko, O.; Breu, J.; Hong, W.; Zheng, Q.; Wu, Z. L. Michell's-instability-mediated fast reconfiguration of hydrogel-based ring actuators. *Adv. Mater.* **2025**, e11239.
33 Zhu, Q. L.; Liu, W.; Khoruzhenko, O.; Breu, J.; Bai, H.; Hong, W.; Zheng, Q.; Wu, Z. L. Closed twisted hydrogel ribbons with self-sustained motions under static light irradiation. *Adv. Mater.* **2024**, *36*, 2314152.
34 Goriely, A. Twisted elastic rings and the rediscoveries of Michell's instability. *J. Elast.* **2006**, *84*, 281–299.
35 Michell, J. H. On the stability of a bent and twisted wire. *Messenger Math.* **1889**, *11*, 181–184.
36 Fullbrandt, M.; Ermilova, E.; Asadujjaman, A.; Holzel, R.; Bier, F. F.; von Klitzing, R.; Schonhals, A. Dynamics of linear poly(*N*-isopropylacrylamide) in water around the phase transition investigated by dielectric relaxation spectroscopy. *J. Phys. Chem. B* **2014**, *118*, 3750–3759.
37 Gomez-Galvan, F.; Lara-Ceniceros, T.; Mercado-Uribe, H. Device for simultaneous measurements of the optical and dielectric properties of hydrogels. *Meas. Sci. Technol.* **2012**, *23*, 025602.
38 Ru, Y. F.; Liu, M. J. Superwetting gels: wetting principles, applications, and challenges. *ACS Nano* **2025**, *19*, 7583–7600.
39 Halperin, A.; Kröger, M.; Winnik, F. M. Poly(*N*-Isopropylacrylamide) phase diagrams: fifty years of research. *Angew. Chem., Int. Ed.* **2015**, *54*, 15342–15367.
40 Bai, H. Y.; Zhu, Q. L.; Cheng, H. L.; Wen, X. L.; Wang, Z. J.; Wu, Z. L. Muscle-like hydrogels with fast isochoric responses and their applications as soft robots: a minireview. *Mater. Horiz.* **2025**, *12*, 719–733.
41 Dai, C. F.; Khoruzhenko, O.; Zhang, C.; Zhu, Q. L.; Jiao D.; Du, M.; Breu, J.; Zhao, P.; Zheng, Q.; Wu, Z. L. Magneto-orientation of magnetic double stacks for patterned anisotropic hydrogels with multiple responses and modulable motions. *Angew. Chem. Int. Ed.* **2022**, *61*, e202207272.
42 Nie, Z. Z.; Zuo, B.; Wang, M.; Huang, S.; Chen, X. M.; Liu, Z. Y.; Yang, H. Light-driven continuous rotating Möbius strip actuators. *Nat. Commun.* **2021**, *12*, 2334.
43 Baumann, A.; Sánchez-Ferrer, A.; Jacomine, L.; Martinoty, P.; Le

Houerou, V.; Ziebert, F.; Kulić, I. M. Motorizing fibres with geometric zero-energy modes. *Nat. Mater.* **2018**, *17*, 523–527.
44 Gelebart, A. H.; Jan Mulder, D.; Varga, M.; Konya, A.; Vantomme, G.; Meijer, E. W.; Selinger, R. L. B.; Broer, D. J. Making waves in a photoactive polymer film. *Nature* **2017**, *546*, 632–636.
45 Zhao, Y.; Liu, Z.; Shi, P.; Chen, C.; Alsaid, Y.; Yan, Y.; He, X. Antagonistic-contracting high-power photo-oscillators for multifunctional actuations. *Nat. Mater.* **2024**, *24*, 116–124.
46 Chen, C.; Liu, Z.; Shi, P.; Zhao, Y.; Duan, S.; Du, Y.; Yan, Y.; Si, M.; Iwasaki, T.; He, X. Bio-inspired multimodal soft actuator with environmental self-adaptation. *Nat. Commun.* **2025**, *16*, 7630.
47 Zang, H.; Liao, B.; Lang, X.; Zhao Z. L.; Yuan W. F.; Feng X. Q. Bionic torus as a self-adaptive soft grasper in robots. *Appl. Phys. Lett.* **2020**, *116*, 023701.
48 Johanns, P.; Grandgeorge, P.; Baek, C.; Sano, T. G.; Maddocks, J. H.; Reis, P. M. The shapes of physical trefoil knots. *Extreme Mech. Lett.* **2021**, *43*, 101172.